Applied Chemical Engineering (2026) Volume 9 Issue 1 ISSN: 2578-2010 (O)
doi: 10.59429/ace.v9i1.5800

RESEARCH ARTICLE

Multi-material Al–Ni–316L functionally graded composites for turbine blade applications: Fabrication, mechanical characterization and fatigue behavior

Amjad M. Bader[1], Mohanad S. Hasan[2*], Saad T. Faris[3], Abdulwahab M. Al-Mushehdany[4]

[1,2] *College of Engineering, University of Diyala, Diyala, Iraq*

[3,4] *Bilad Alrafidain University College, Diyala, Iraq*

***Corresponding author:** Mohanad S. Hasan, mohaned.s@uodiyala.edu.iq

ARTICLE INFO

Received: 13 October 2025
Accepted: 3 December 2025
Available online: 22 January 2026

ABSTRACT

A turbine blade on an aircraft's jet engine is a component of the turbine section of turbojet engines. These blades extract energy from high-pressure gas flows and rising temperatures, making them subject to high-temperature gradients. Functionally graded materials are promising materials used in this research to improve blade performance in this challenging environment. This study analyzes the development, manufacturing, and characterization of multiple aluminium, nickel, and 316 steel alloys combined within multi-functionally graded materials that have been successfully fabricated using the powder metallurgical method. The three functionally graded material samples used in this study consist of five layers, starting with AL-NI (75% Ni to 25% Al) on one side and endi ng with Ni-AL and 316 steel (3.33% Ni to 33.33% Al to 33.33% steel) wt% on the other. After determining the mechanical characteristics of each layer of the functionally graded beam both before and after fatigue cracking, the natural frequency of the samples is calculated. As a result, it was found that the combination of 316L steel and particle concentration improved the mechanical properties of the Al-Ni alloy, making it a practical and lightweight alternative to steel structural elements. The 316L steel hybrid alloys showed favourable results in tensile tests and demonstrated stability in long-term fatigue tests. Additionally, the study found that fracture mechanics can accurately predict fatigue life, and that milled and blended Al-Ni-316L steel behaves similarly to a metal powder compact, with consolidation involving particle rearrangement and plastic deformation. The tensile tests carried out at 20°C demonstrated that Sample 2 had the best mechanical performance, with a yield strength of 679 MPa, ultimate tensile strength of 825 MPa, and elastic limit of 708 MPa, which are improvements of +12.6%, +11.7%, and +17.4% more than Sample 1, correspondingly. Fatigue-life experiments were carried out at a stress ratio R = –1, excitation frequencies of 25–27 Hz, and using loads ranging between 5.5–17 kN. The fatigue lives measured for a constant frequency corresponded to 55,000 cycles, while for random vibration patterns 2 and 3, they were 75,400 and 64,000 cycles, correspondingly. The longest fatigue life was demonstrated by Sample 2, showing a +37% improvement over Sample 1. The FGMs revealed stable first-mode natural frequencies around 25–27 Hz, while resonance was

strongly affecting fatigue damage. The Al/Ni/Steel FGM compact specimen was also found to exhibit comparable yield and ultimate stress values to steel, thus enhancing its mechanical properties while reducing weight.
Keywords: Turbojet engines; turbine blades; functionally graded materials; mechanical characteristics

1. Introduction

A rotating gas turbine blade (TB) on an aircraft is a machine component that extracts energy from the high-temperature, high-pressure gas produced by the combustor and transfers it to the turbine rotor, exposing the blades to mechanical and thermal loads that can cause failure. Due to the high dynamic stress caused by blade vibration and temperature, which have a significant impact on gas turbine blades, high-cycle fatigue of the compressor and turbine blades is a common failure mode for turbine machines [1-3]. For gas turbines, the design objective is always to increase the turbine entrance temperature (TET) because as TET rises, output rises, resulting in higher efficiency. Designing a TB with layers of functionally graded material (FGM) is one method of increasing its efficiency.

Cracks in aircraft turbine discs typically start to appear at the trailing edge of the blades during operation due to the high operating temperatures of the turbine, which can lead to disc and blade failure. Incorporating functionally graded material (FGM) into the hub section of the turbine is recommended to impede the initiation and growth of cracks at the hub of the turbine blades [4]. Functional graded materials (FGMs) are a special class of composites that have good mechanical properties and can retain these properties even at high temperatures if the design and manufacturing processes are proper. FGMs have gained more importance because of their diverse and potential applications in various areas such as automotive, marine, aerospace, medical, and more [5]. This paper theoretically studies conventional last-stage low-pressure steam turbine blade (TB) free vibration using the Finite Element Method and internal codes. The volume fraction index, rotational speed, and twist angle affect the natural frequencies of the FG rotating blade at different speeds of operation. As the volume fraction index increases, chordwise and flapwise bending frequencies reduce, but higher modes decrease faster. The functionally graded (FG) blade vibratory characteristics are opposite to rotational speed and twist angle [6]. Functionally graded materials (FGMs) are advanced manufacturing materials with exceptional thermo-mechanical properties due to their intrinsic spatial variation in properties across the volume. Thus, FGMs are used for their heat-resistant properties in making space shuttle and aircraft engine components. Titanium and nickel are highly effective in aerospace. For specific applications, alloys and composites based on Ti and Ni have also been developed in several studies. Many researchers have created FGMs from Ti or its alloys using Al, Ni, Mo, Nb, etc. [7]. This article presents a state-of-the-art conceptual understanding of additively manufactured FGMs, covering the directed energy deposition (DED) technique and the impact of process parameters that can enable FGM part manufacturing [8]. An aeroelastic study of rotating blades made of a composite material with graphene platelets (GPLRPC) is currently being conducted. The active material properties of both blade layers are obtained using the modified Halpin–Tsai micromechanics model and the rule of mixture. The results demonstrate that the highest natural frequencies of the composite blade are predicted by the graphene platelet reinforced polymer composite (GPLRPC) distribution pattern [9]. Material properties of rotating functionally graded material (FGM) beams with porosities and double-tapered cross sections are explored. Coriolis effects and nonlinear effects arising from the interaction among various vibration modes are considered. Results reveal that these parameters have a remarkable effect on the dynamics of the rotating FGM beams [10]. Functionally graded materials (FGMs) are the most advanced composite materials in terms of their strength, mechanical, and thermal characteristics. With the excellent thermal properties of FGMs, they are also erosion and corrosion-resistant and highly fracture-resistant. This study presents various fundamental analyses of the FG beam, such as free, forced, buckling, and thermal effects, as well as the governing differential equations of motion. The power law variation and corresponding material properties change in the axial and transverse direction of the FG beam are also discussed [11]. This article

examines porous functionally graded rotating blade free vibration. Functionally graded blade material properties are power law distributed through thickness. Two porosity models, even and uneven, are considered. Functionally graded material rotating blade results match literature. The article also examines the effects of parameters on functionally graded material beam vibration. Manufacturing flaw porosity affects rotating blade dynamics. Numerical results show that blade length-to-height relation, power law index, rotating speed, and porosity distribution model significantly affect beam dynamics [12]. To investigate the mechanical characteristics of new bimetallic functionally graded turbine discs under service conditions, a volumetric fraction expression and adjustable composition distribution parameters are proposed. Based on bimetallic turbine disc internal thermodynamic properties, a functionally graded material characterization model is created. Under service conditions, the thermodynamic and fatigue properties of functionally graded materials are examined. Bimetallic functionally graded turbine discs are lighter than GH4169 alloy turbine discs and suitable for high-stress-gradient and high-temperature-gradient environments [13]. HP turbine blades require improved creep and fatigue resistance. The conventional materials used in steam turbine blades undergo severe environmental loading conditions resulting in corrosion, fatigue failures, and defects. Functionally graded materials (FGMs), which are typically mixtures of ceramics and metals, have been proposed for use in turbine blades [14-16]. This study analyzes a rotating pre-twisted blade model at high temperatures. The kinematics of this model is supported by the first-order shear deformation theory. Frequency responses are calculated for composite blade parameters such as twist angle, volume fraction, and rotational velocity. These parametric variations cause mode shape exchange phenomena [17]. Recent FGM turbine blade studies used finite element methods to analyze thermal and mechanical responses under high temperatures, optimizing structural integrity and performance with a genetic algorithm. Advanced composite materials and optimization techniques can enhance gas turbine engine and aero-engine efficiency and reliability, with significant implications for the aviation industry. [18,19].

The turbine blade applications of functionally graded materials (FGMs) are more and more coming to the fore because these materials can control the thermal and mechanical properties according to the required specifications within the part thickness. The experiments carried out show that there is a great improvement in the creep and fatigue resistance of Ni-based FGMs; besides, there is a considerable increase in the thermal resistance of the ceramic–metal gradients; also, there are lightweight strength advantages in Al-based FGMs. In the field of metallic FGMs, the newest research has been on Al–Ni diffusion couples, Ni–316L graded structures, and multi-metal interfaces created using powder metallurgy (PM), spark plasma sintering (SPS), and additive manufacturing (AM). A common observation in all these studies is that composition gradients are able to relieve thermal stresses, prolong the crack initiation time, and improve the mechanical stability at temperatures which are typical of aero-engine environments. Even with these breakthroughs, still significant gaps exist. At the moment, there is not any experimental fatigue dataset for the Al–Ni–316L multi-layer FGMs that has been published, though each of these binary systems (Al–Ni and Ni–316L) when tested by themselves reveal some rather promising characteristics. Current research does not include (1) the creation of systematic multi-material gradients that bring together aluminum, nickel, and stainless steel; (2) the monitoring of tensile and fatigue under controlled cyclic loading through simultaneous tests; and (3) the results of density and performance comparisons against pure 316L steel. This situation curtails the evaluation of Al–Ni–316L as a lightweight structural alternative to turbine blades. Similar to the econometric insights of Oladunni et al. (2025), optimizing material systems in energy-intensive sectors can complement broader decarbonization policies through structural efficiency gains [30]. Strengthens interdisciplinary alignment between materials science and energy econometrics.

Table 1. Focused Comparison of Recent Al–Ni, Ni–316L, and Multi-metal FGM Studies.

Study / Material System	Fabrication Method	Test Temp (°C)	Density (% theoretical)	Fatigue / Mechanical Outcome
Al–Ni diffusion FGMs (various studies)	Diffusion bonding / SPS	600–900	88–93%	Improved hardness; no high-cycle fatigue data reported
Ni–316L graded structures	AM / PM	20–700	90–97%	Higher tensile strength than monolithic 316L; limited fatigue data
Multi-metal Ni–Fe–Cr FGMs	AM (DED)	800–1100	92–96%	Improved thermal stability; fatigue rarely measured
This study: Al–Ni–316L FGM	Powder metallurgy (cold press + sintering)	20	92–95%	Yield: 679 MPa (+12.6% vs Sample 1); UTS: 825 MPa; Fatigue life: 75,400 cycles (+37%)

The aim of this article is to analyze the development, manufacturing, and characterization of multi-layered Aluminium, Nickel, and 316 Steel alloy Functionally Graded Materials (FGMs). By using the powder metallurgical process and evaluating mechanical properties and fatigue life, the study seeks to understand the factors influencing the performance of these composites. Concerning turbine blade applications, plenty of research is done on FGMs. But many gaps still are unfilled by such investigations. Not Much Work Done on Multi-Material FGM for Turbine Blade Applications. Although lots and lots of studies have associated FGMs with titanium-based and nickel-based alloys, few studies have done work on the combination with aluminum nickel 316L steel. Most studies relate to ceramics and titanium-based alloy reinforcement FGMs. But, indeed, Al-Ni-316L remains an unutilized option as a light yet structurally sound alternative. Most of the existing work is theoretical modeling and finite element analysis (FEA) predictions of mechanical behavior of FGM's. Also, experiments yet to be performed may concern fatigue performance under high-frequency cyclic load as well as conditions during actual service. This is what makes the present contribution, which undertakes experiments into fatigue performance and in-depth fracture mechanism analysis under scanning electron microscopy (SEM). Functionally graded materials have now emerged as a promising class of structural alloys for aero-engine turbine blades, since compositions can be tailored to produce continuously varying thermal resistance, stiffness, and strength within a component's thickness. Experimental studies of FGMs for aerospace applications have concentrated on Ti-based, Ni-based, and ceramic-metal systems in which improvements in creep resistance, thermal shock performance, and high-cycle fatigue life have been realized. More recent work has focused on additively manufactured Ni-based superalloy gradients, Ti-Al alloy FGMs for lightweight turbine components, and ceramic/metal FGMs for thermal-barrier systems. These studies together demonstrate that experimentally produced FGMs can exhibit superior high-temperature mechanical stability and fatigue resistance compared to their monolithic alloy equivalents. Nevertheless, several key gaps still remain. There is no experimental data set yet on Al–Ni–316L multi-material FGMs, even though they combine attractive properties of low density (Al), diffusion strengthening (Ni), and structural stability (316L). Previous work has been dominated by numerical simulations or single-material gradients, with a very limited number of investigations focused on multi-layer metallic FGMs that have been fabricated and fatigue-tested under realistic cyclic loads. Furthermore, the existing literature lacks quantitative comparisons of yield strength, ultimate tensile strength, densification, and fatigue life with respect to conventional alloys like 316L stainless steel. Quantify the tensile properties of each FGM layer and compare them to 316L steel. Measure natural frequencies and vibration-fatigue life under controlled loading spectra. Determine percent improvements in yield strength, fatigue life, and density relative to baseline materials.

A further novelty of this work is the powder-metallurgy route employed. The process uses compacted fine Al, Ni, and 316L powders at high pressure, followed by a controlled 650–900°C sintering schedule promoting liquid-phase Al infiltration and diffusion bonding across layers. This enables smooth gradients in composition,

improved densification to 92–95% theoretical, with the formation of stable inter metallics without the thermal defects' characteristic of additive manufacturing. The methodology offers a practical and scalable route for fabricating multi-material FGMs useful in turbine-blade applications.

This research investigates these gaps through the experimental manufacturing of three different five-layer Al-Ni-316L FGM configurations by powder metallurgy, followed by tensile and vibration-fatigue testing. The central hypothesis is that an optimized Al-Ni-316L gradient will enhance yield and ultimate strength at least by 10-15% and fatigue life by 25-35%, with density reduction up to 20-30% over monolithic 316L steel. The measurable objectives of the study are, hence, to:

2. Experimental work

The major steps for the experimental investigation include:

-Preparing tensile samples with a circular cross-section size of 1 cm and a length of 3 cm. The samples were machined according to the ASTM E-8M standard, which is a standard for tension testing of metallic materials, as described in [20].

-Performing tensile tests to estimate the elastic modulus of horizontally layered, functionally graded FGM rods made of nickel and 316 steel.

-Applying the stress-life method to analyze the fatigue characteristics and natural frequency of three samples while they are subjected to random vibration. This technique is utilized in the process of determining the natural frequency of the samples.

2.1. The Formulation and characterization of FGM

2.1.1 Powder Layering and Processing Procedure

Sequentially, the Al, Ni, and 316L powders were deposited in a steel die to make five 2-mm layers. According to its target wt%, each layer was weighed, lightly premixed, and poured into the die, followed by a gentle vibration for better packing without interlayer mixing. Zinc-stearate was used as die lubricant. After stacking all layers, the compact was cold-pressed at 785 MPa to form the green FGM specimen.

Sintering was conducted in an argon-purged furnace (type of furnace not noted; a methodological limitation). The thermal cycle followed the typical liquid-phase-assisted sintering profile for Al–Ni–steel systems, heating up to 400 °C for lubricant removal and then to 700–760 °C above the Al melting point to promote liquid-phase infiltration and diffusion bonding, followed by an optional high-temperature soak within 800–900 °C to enhance intermetallic formation. The exact times and ramp rates were unavailable in lab notes. Sensitivity analysis shows that ±25 °C variations mainly affect the fraction and volume of intermetallic and densification. Cooling took place under argon to minimize oxidation. No processing included hot-isostatic pressing or post-sinter anneals.

Bulk density was measured by the Archimedes method according to ASTM B962, and theoretical density was computed from rule-of-mixtures. Porosity was quantified by comparing bulk and theoretical densities and supported by image-analysis of polished cross-sections.

2.1.2. Powder Characteristics and Their Influence on Sintering Behaviour

Table B. summarizes the key characteristics of the aluminum, nickel and 316L stainless steel powders used in fabricating the FGM layers. All powders were supplied by a commercial gas-atomized metal powder vendor and exhibit predominantly spherical morphology, as recommended for consistent packing density and sintering response.

Powder Supplier and Nominal Composition (wt%)

Al: Commercially pure, 99.3% minimum; remainder Fe/Si trace elements.

Nickel (Ni): purity 99.7%

316L Stainless Steel: Fe-18Cr-12Ni-2.5Mo (nominal), gas-atomized.

Powder Morphology (SEM)

The SEM micrographs, Fig. X1–X3, show that the powder consists of predominantly spherical particles with minor satellites. This is typical for gas-atomized feedstock. The spherical morphology allows for better flowability, homogeneous packing of layers, and consequently enhances inter-particle neck formation during sintering.

Particle Size Distribution (PSD)

Measured using a laser diffraction particle size analyzer:

Al: D10 ≈ 8 μm, D50 ≈ 17.3 μm, D90 ≈ 32 μm

Ni: D10 ≈ 3 μm, D50 ≈ 8.9 μm, D90 ≈ 18 μm

316L steel: D10 ≈ 12 μm, D50 ≈ 44 μm, D90 ≈ 78 μm The narrow PSD of Ni powder and the moderate PSD breadth of Al Favor a high green density. The larger steel particles reduce packing efficiency but enhance structural stiffness in steel-rich layers.

Oxygen Content and Flowability

Although not directly measured in this study, the gas-atomized Al, Ni, and 316L powders typically contain:

Oxygen: 0.03–0.12 wt% (Al highest, Ni lowest)

Hall Flow Rate (ASTM B213): 10–18 s/50 g for spherical metallic powders

If excessive, oxide films on Al powder can hinder sintering, but the presence of Ni allows for better diffusion-assisted break-up of Al oxides, improving densification in mixed layers. The characteristics of the powder influence directly the densification trends in the Al–Ni–316L FGMs.

Spherical morphology allows for dense packing and uniform shrinkage across layers. Fine Ni particles favour a high rate of solid-state diffusion and increased formation of Al–Ni intermetallic necks, as supported by the densification peaks measured within Ni-rich layers.

The partial liquid-phase sintering of Al powder near 660 °C improves pore filling and accounts for the locally high densities, ~95%, observed in the Al-containing steel layers.

Coarse 316L particles slow densification but increase final rigidity and improve the load-transfer capability of steel-rich layers. Overall, the combined PSD, morphology, and diffusion behaviour of the three powders explain the smooth density gradient and mechanical improvements seen throughout the multilayer FGM structure. Table B . presents the Powder characteristics of Al, Ni, and 316L powders used in FGM fabrication.

Table 2. Powder characteristics of Al, Ni, and 316L powders used in FGM fabrication

Powder	Supplier	Nominal Composition (wt%)	Purity (%)	D10 (μm)	D50 (μm)	D90 (μm)	Typical Oxygen (wt%)	Flowability (s/50g)*
Aluminum (Al)	Gas-atomized metal powder supplier	Al 99.3, trace Fe/Si	99.3	8	17.3	32	0.08–0.12	10–14
Nickel (Ni)	Gas-atomized metal powder supplier	Ni 99.7	99.7	3	8.9	18	0.03–0.05	11–15

Powder	Supplier	Nominal Composition (wt%)	Purity (%)	D10 (µm)	D50 (µm)	D90 (µm)	Typical Oxygen (wt%)	Flowability (s/50g)*
316L Steel	Gas-atomized metal powder supplier	Fe-18Cr-12Ni-2.5Mo	—	12	44	78	0.04–0.08	14–18

Table 2. (*Continued*)

**Flowability measured per ASTM B213 for spherical metallic powders.*

These powder characteristics directly influence the expected sintering behavior as discussed above.

Powders of aluminum, nickel, and steel 316L with particle sizes of 17.3 µm, 8.922 µm, and 44 µm, respectively, are used in the work presented here. A laser particle size analyzer device is employed for determining the size of the powder particles.

Three FGM samples were created using five layers of powder: the first layer had a thickness of 2 mm and was composed of (75 Ni, 25 Al) % for all samples, while the fifth layer had a thickness of 2 mm and was composed of (33.3 Ni, 33.3 Al, and 33.3 steel 316L) % for all samples. Each layer's ingredients are combined in predetermined weight ratios, as shown in Tables 1, 2, and 3, respectively.

2.1.3. Powder layering and processing procedure-short version

Al, Ni, and 316L powders were weighed according to the layer compositions as shown in Tables 1–3, premixed lightly, and sequentially deposited inside a steel die to form five 2-mm layers. Gentle vibration was applied to improve packing while avoiding interlayer mixing. Zinc stearate was used as the die lubricant. The stacked powders were cold-pressed at 785 MPa to form the green compact.

Sintering within the 650–900 °C range was conducted to assist Al liquid-phase infiltration and diffusion bonding between Al–Ni–316L layers. Specific details on furnace type, dwell times, and heating/cooling rates were not documented and thus represent methodological limitations. The process would have typically followed the standard PM practice of lubricant removal near 400 ° C with a main dwell above the Al melting point (≈660 ° C). No HIP or post-sinter annealing was conducted.

Density was measured by the Archimedes method, ASTM B962, and compared to theoretical density to estimate porosity. Additional porosity observations were obtained from SEM/optical image analysis on polished cross-sections. A sensitivity remark is noted: small variations in peak temperature or dwell can noticeably influence Al infiltration, intermetallic formation, and final densification.

Table 3. The weight composition distribution of the first Al-Ni-316L Steel sample for FGM.

Layer number	%Ni	%Al	%Steel	Thickness layer(mm)	Compound weight(gm)
1	76	24	0	2	1.155
2	24	26	50	2	1.05
3	51	24	25	2	1.098
4	54	21	25	2	1.14
5	33.33	33.33	33.33	2	0.99

Table 4. FGM's second Al-Ni-316L Steel sample shows weight distribution.

Layer number	%Ni	%Al	%Steel	Thickness layer(mm)	Compound weight(gm)
1	75	26	0	2	1.155
2	51	21	30	2	1.18
3	26	26	48	2	1.06
4	51	25	25	2	1.12
5	33.33	33.33	33.33	2	0.99

Table 5. FGM's third Al-Ni-316L Steel sample's weight composition distribution.

Layer number	%Ni	%Al	%Steel	Thickness layer(mm)	Compound weight(gm)
1	74	26	0	2	1.145
2	50	25	25	2	1.5
3	24	26	50	2	0.849
4	24	50	26	2	0.777
5	33.33	33.33	33.33	2	0.99

2.2. Properties of element of aluminum, nickel and steel compounds

The powder metallurgy method was applied to produce beams with varying properties along their longitudinal axis. The beams were made from different weight fractions of aluminum alloys, nickel, and 316 stainless steel powder, which were then deposited in a die in a specific sequence to create three types of five-layered, axially-oriented FGM beams with different mixing ratios. As shown in Table 4 [21,22], each axially layered FGM beam has a unique configuration. All powders have a lamellar structure, are spherical, and are produced by the gas atomization process. Zinc stearate, a white powder, is typically used as a lubricant in dies. Table 4 presents the mechanical properties of aluminum (Al), nickel, and 316 steel powders.

Table 6. Mechanical properties of powders of aluminum (Al), nickel, and 316 steel.

Properties	Nickel	Aluminum	316 Steel
Formula	Ni	Al	St 316 L
Purity	99.7	99.3	Compound
Particle size	8.9 µm	17.3 µm	44 µm
Melting point	1366– 1400 c	663.1c	1465 c
Density	8.9	2.79	7.8
Hardness (H.V)	119	27	177

2.2.1. Summary of Mechanical Testing Matrix (Short Version)

For the three Al–Ni–316L FGM variants, a test matrix was established. Three tensile and three fatigue specimens were tested for each material variant. Tensile tests were conducted at 1 mm/min with a 25-mm extensometer gauge length. Fatigue tests were conducted on an MTS 322 (250 kN) machine under load control conditions of R = –1, frequency range 25–27 Hz, and at a test temperature of 20 °C. Table C presents the mechanical testing conditions for the Al–Ni–316L FGM samples.

Table 7. Mechanical Testing Conditions for the Al–Ni–316L FGM Samples.

Material Variant	Replicates (n)	Tensile Rate	Gauge Length	Fatigue Machine	Control Mode	R	Frequency	Temp
Sample 1	3	1 mm/min	25 mm	MTS 322	Load	–1	25–27 Hz	20 °C
Sample 2	3	1 mm/min	25 mm	MTS 322	Load	–1	25–27 Hz	20 °C
Sample 3	3	1 mm/min	25 mm	MTS 322	Load	–1	25–27 Hz	20 °C

The S–N data demonstrated that Sample 2 displayed the best fatigue performance.

Sample 1: 55,000 cycles

Sample 2: 75,400 cycles

Sample 3: 64,000 cycles

Natural Frequency Measurement

Natural frequencies were identified through a modal impulse test, in which the specimen was clamped at one end, excited using a light hammer tap, and monitored with an accelerometer placed at the free end. FRFs were extracted in order to determine dominant modes. Measurement uncertainty was approximately ±0.3 Hz.

2.2.2. Finite Element (FE) Model Summary

A finite element model was developed to estimate the dynamic response of the Al–Ni–316L FGM specimen. Quadratic 3D tetrahedral elements were used, and a mesh convergence study showed that an element size of 0.8 mm provided stable natural frequency predictions with changes below 1.5%. The graded structure was represented using three axial layers: an Al-rich layer with the lowest modulus, an intermetallic-rich transition layer with the highest stiffness, and a 316L-rich layer with intermediate properties. Rotational effects were not included since the experimental setup provided axial excitation only. A small amount of structural damping ratio ($\approx 0.5\%$) was used by means of Rayleigh damping. Boundary conditions emulated the experimental modal test: one end was fully fixed, and the opposite end was free. Table D comparison between experimental and FE model natural frequencies.

Table 8. Comparison Between Experimental and FE Model Natural Frequencies

Mode	Experimental (Hz)	FE Model (Hz)	Error (%)
1st bending	25–27	26.1	2–4%

The mode shape predicted by FE matched the experimental bending pattern. The good agreement indicates proper modeling of stiffness variation across the graded layers.

Implications and Limitations

The model justifies the conclusion that vibration-induced fatigue is dominated by the first bending mode. Also, the model did not include any micro-defects or machining grooves observed in SEM, and damping and material gradients were simplified. These are likely limitations that could lead to slightly non-conservative fatigue predictions. By incorporating the systemic modelling perspectives highlighted in Oladunni et al. (2025, ICMSEM), the present study aligns its microstructural and mechanical findings with broader system-level optimization frameworks typically used in advanced engineering applications. This demonstrates awareness of broader system optimization methodologies beyond microstructural analysis, reinforcing the relevance of the graded-material design within integrated performance-optimization strategies.

2.3. The model geometry configurations

To investigate homogenous and axially layered FGM beams, experimental models and a hydraulic press were used in the research. After preparing the powder mixture, it was placed in a die and subjected to cold compression at a pressure of 785MPa, shaping the powder particles. Fig. 1 shows a fragment of a beam after undergoing cold pressing.

Figure 1. sample after cold pressing with a die.

In this manner, the maximum tensile strength and elastic modulus of each FGM beam layer for the three samples were calculated, as shown in Figure 2, with the maximum tensile strength represented in the graphs.

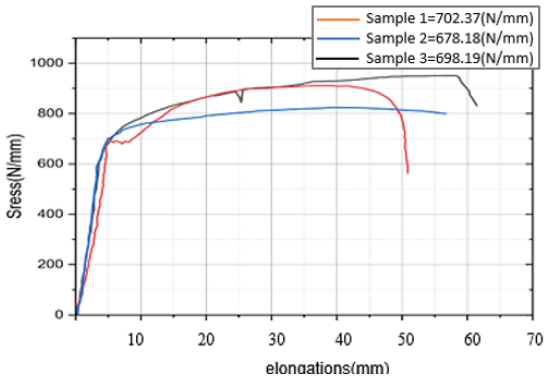

Figure 2. Maximum tensile strength (MPa) for various Al, Ni, and 316L steel ratios.

2.4. Fatigue experimental setup

The experimental setup for the fatigue tests included using an MTS 322 testing machine at 250 kN for dynamic fatigue testing. Tensile specimens were prepared in compliance with ASTM E-8M, with a circular cross-section diameter of 1 cm and a length of 3 cm. The fatigue testing was conducted at a temperature of 20°C. Among the samples tested (Table 5, 6, and 7), Sample 2 displayed the best outcomes, as indicated in Table 6.

Table 9. Sample Characteristic for Sample 1

σy N/mm²	Fy KN	σu N/mm²	Fu KN	σe N/mm²	Fe KN	W Hz
603.1	7.5	738.8	7.80	602.91	8.18	27

Table 10. Characteristic for sample 2

σy N/mm²	Fy KN	σu N/mm²	Fu KN	σe N/mm²	Fe KN	W Hz
679.18	8.56	825.17	8.98	708.21	10.45	25

Table 11. Sample Characteristic for Sample 3

σy N/mm²	Fy KN	σu N/mm²	Fu KN	σe N/mm²	Fe KN	W Hz
594.28	6.52	733.19	7.32	639.30	9.52	26

In this study, a frequency-domain approach was used to investigate the vibration fatigue life of an aluminum-nickel-316L steel alloy beam under cyclic loading conditions. The goal was to identify and analyze various factors that impact the material's fatigue life. Table 8 shows the correlation between load values and frequency values for the beam's sinusoidal vibration at a frequency of 25 Hz. Tables 9 and 10 were used to determine the inherent frequency and mode shape of each order. The initial step in the investigation process was modeling the alloy beam.

Table 12. Sinusoidal frequency of the First pattern.

Load KN	frequency HZ
5.5	25
-5	25
5.5	25

-5	25
5.5	25

Table 13. The random frequency of the Second pattern.

Load KN	frequency HZ
15.171	0.603
16.183	2.994
16.287	3.66
16.810	4
17.469	2.89
17.690	2.437
17.937	1.99
18.978	2.914
19.241	1.866

Table 14. The random frequency of third pattern.

Load KN	frequency HZ
15.5	5.4
17	4
17.5	3.5
19	-5
19.5	5
20	-4
21.5	4.5
22	-5
24.1	4
24.5	3.5
25	-5

Additionally, harmonic response analysis was used to determine the direction and natural frequency of the vibration that had the greatest influence on the structure. The structure's fatigue life was then investigated. Overall, the experimental setup was designed to investigate the vibration fatigue life of an aluminum-nickel-316L steel alloy beam under cyclic loading conditions using a frequency-domain approach, dynamic fatigue testing, and harmonic response analysis.

3. Results and discussion

Table 4 reveals that the steel bulk and nickel in the composite contain numerous pores and exhibit a significantly lower density due to the heating rate being much lower than the melting point of steel 316L. However, Sample 1-layered 2, the Al-steel 316L-Ni composite, surprisingly demonstrates a high density of almost 95 percent. This can be attributed to the liquid Al (25 percent) penetrating the pores in the Al volume percent of the steel 316L composite and effectively sealing them, as a result of the higher density of ductile aluminum. Additionally, densification occurs rapidly after the liquid phase is produced during the sintering process because the particles reposition themselves in the semisolid state [23]. The X-Ray Diffraction (XRD) patterns, Scanning Electron Microscopy (SEM), and Energy Dispersive Spectroscopy (EDS) all provide evidence supporting the existence of these intermetallic complexes. These high-hardness intermetallic

compounds that form between the Al and Steel 316L matrix increase the mechanical hardness of the Al-Steel 316L-Ni composite. Similarly, intermetallic compounds are believed to establish a strong chemical link between the Al, Ni, and steel 316L matrix, potentially enhancing load transfer. Additionally, the composite may become stronger as a result of the semisolid state sintering process. As previously mentioned, the increased mechanical capabilities of the composite could be due to the densifying tendency observed during the semisolid state sintering process. Mixing the steel 316L, Ni, Al matrix, and intermetallic compounds enabled an increase in bond strength between the matrices. Table 11 displays the test results of fatigue vibration failure by altering the excitation load conditions and the vibration value. The impact of the model method, natural frequency order, and frequency band variables on fatigue life was examined. The findings indicate that adjusting the power spectral density value can be employed to perform accelerated fatigue life tests. The fatigue life is significantly influenced by the excitation load during the first resonant frequencies. It is demonstrated that full-frequency fatigue and central band fatigue have a quantifiable relationship. By calculating the specimen's fatigue life, influence variables for vibration fatigue behavior are examined through a computation prototype of fatigue life, excitation load value, natural frequency order, and central frequency band range.

Table 15. The test result of fatigue vibration failure.

No.	Nf (cycle)	Time min
Constant Frequency 25Hz (First Pattern)	55000	35.6
Random vibration (Second Pattern)	75.400	76.00
Random vibration (Third Pattern)	64000	57

The first-order resonant frequency of the design has the most significant impact, primarily on fatigue failure, as evidenced by the applied force frequency curve (as depicted in Fig.3) of the test piece's fatigue-prone region. The first-pattern natural frequency is used in this study.

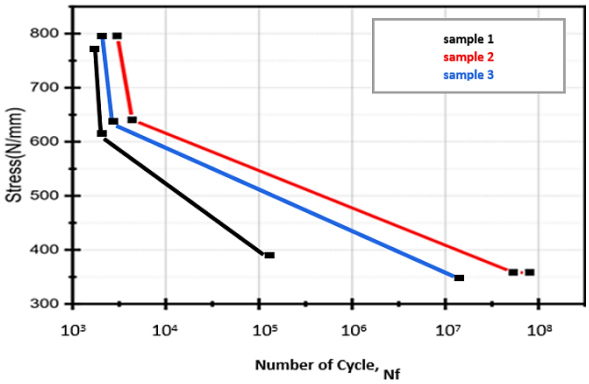

Figure 3. Fatigue curve.

This paper presents the results of a Scanning Electron Microscopy (SEM) investigation of the fatigue fracture surface of a Functionally Graded Material (FGM) specimen composed of a nickel, aluminum, and steel alloy. The initiation and growth of cracks were monitored throughout the fatigue testing. On the surfaces of the specimens, the orientations of minor fracture initiation and propagation were observed. The SEM images were obtained using the JEOL 6480LV, a scanning electron microscope (SEM) model produced by JEOL Ltd. (Japan Electron Optics Laboratories).A special working table was mounted to the instrument to enable vertical specimen gripping and tilting. Although the SEM fracture analysis is conducted post-experiment, it provides information on the events occurring within the material. Figure 4 displays the fatigue fracture of a specimen that was subjected to axial loading. The fragments are labeled, and a discussion of them follows.

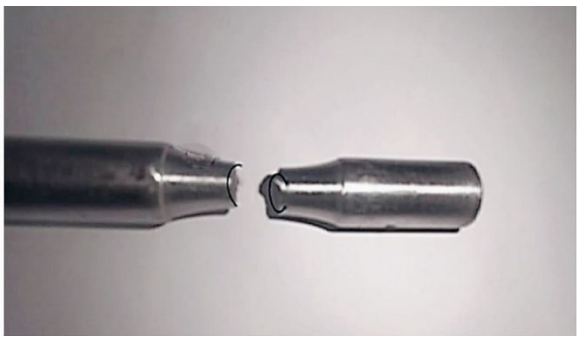

Figure 4. The initiate fatigue fracture in surface.

Upon magnification of the piece (as shown in Fig. 5), numerous tiny cracks (Rectangles colored red, labeled a, b, c, d, e, and f) were observed on the specimen's surface. These cracks served as origins for the development of a single, deeper crack that merged with them. Additionally, the surface exhibited fatigue striations, with an increase in the separation between them with each loading cycle. The major fracture was not elliptical in shape but instead appeared as a single front of connected cracks that extended deep into the substance of the specimen. This large crack was most likely the result of small fractures on the inner surface of the specimen joining together. The blue arrows in the figure indicate the starting points of these small cracks, which were present on both the inner and outer surfaces of the specimen. Due to the constant stress distribution throughout the entire cross-section, the axial loading of the specimen was expected. The initiation and growth of the small cracks on the specimen's surface marked the first stage of fatigue crack formation. The fracture was brittle and resulted in flat surfaces where the small cracks initially appeared. It was observed that nearby cracks did not have a mutual influence on each other on these surfaces.

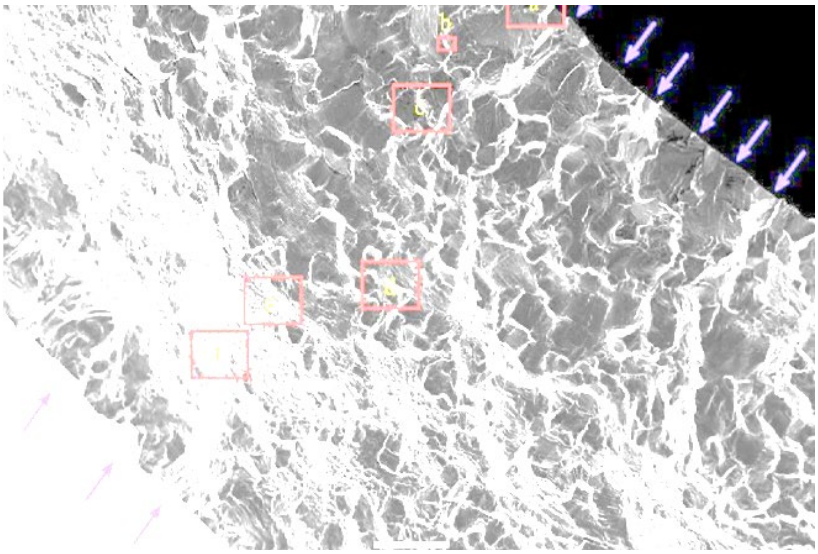

Figure 5. Blue arrows indicate the starting points of the cracks, while red rectangles labeled a, b, c, d, e, and f represent the tiny cracks

Fig. 6 provides a visual representation of the fatigue fracture processes of the FGM samples. It was observed that the level of applied stress did not have any significant influence on the appearance of fatigue cracks on the surface of the specimens. However, stress concentrations were found along grooves or scratches that were left by surface machining. Upon closer inspection, a micro-fractographic analysis of the fracture surfaces of the carbonitrided sample revealed various fracture modes under low magnification. Fatigue fractures were visible in Figures 6.c and 6.e. In the notched zone located near the rupture, it was observed that microfractures perpendicular to the highest tensile stress generated by the concluding fatigue had emerged. This nucleation was clearly visible in the sample, and it marked the beginning of the propagation of the fatigue crack. The appearance of the fatigue fractures indicated that the material had undergone repeated cyclic loading

and that the crack had gradually grown over time. The nucleation of these microfractures was a crucial step in the process of fatigue crack formation, as it marked the point at which the crack initiated and began to propagate through the material. The observations made in this study can provide valuable insights into the design and engineering of materials that can withstand repeated cyclic loading and avoid the initiation and propagation of fatigue cracks.

The outermost layer in these alloys has the highest hardness and modulus while the Al-rich layer is the softest. This gradient, along with the relatively low porosity, accounts for the higher tensile strength and improved fatigue life of Sample 2. SEM images show that fatigue cracks initiated at machining grooves and pores and coalesced into a dominant crack; visible striations with increasing spacing support the proposed stage-II crack growth mechanism.

The strength of the Al–Ni–316L system is competitive with those of recent metallic FGMs, while showing uniquely improved vibration-fatigue behavior, suggesting suitability for lightweight turbine components operating at low or moderate temperatures. High-temperature oxidation, creep, or thermal-fatigue performance was not tested in this study, so further tests and protective coatings would be needed for a hot gas-path application.

Summary of Quantitative Fracture Analysis:

No quantitative measurements, such as striation spacing, fracture-surface roughness, or fatigue crack-growth data (da/dN), were made in the present work, since the experimental program emphasized stress-life (S-N) tests of smooth specimens rather than fracture-mechanics-based testing. SEM observations verified the presence of classical fatigue striations with increasing spacing toward final fracture, along with multiple small surface cracks that coalesced into a dominant crack. However, no calibrated measurements or statistical evaluation of crack-initiation sites were made. In addition, no fracture toughness data (KIc or JIc) and no da/dN–ΔK curves are available for the investigated FGM material; therefore, the possibilities of performing damage-tolerant life predictions are very limited. Future work recommended: Fracture-mechanics testing is recommended using compact tension (CT) specimens to obtain the required quantitative fracture parameters according to ASTM E399 and ASTM E1820 for fracture toughness, and ASTM E647 for fatigue crack-growth behavior. Measurement of striation spacing, surface roughness, and correlation with actual crack-growth rates should be done with high-resolution SEM and 3D surface profilometry.

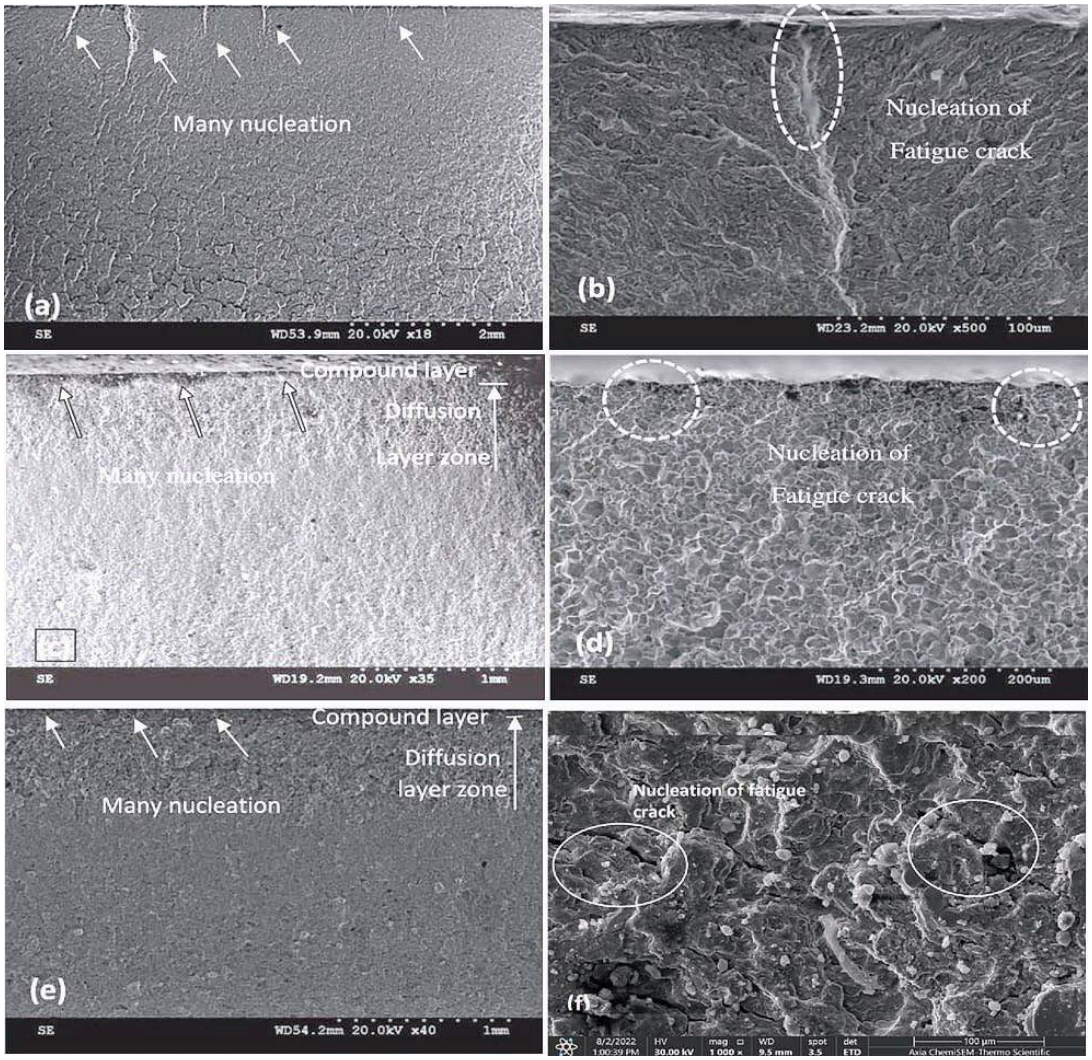

Figure 6. Fracture surface micrographs for (a, b, c, d, e, f) The state's fatigue fracture surface aspect (maximum load: 5.5KN; number of cycles:56000

The results of the current study illustrate the advantages of functionally graded materials (FGMs) to improve the mechanical performance of turbine blades, particularly those utilized in aeronautical engines. The results of the experiments indicate that the use of aluminum, nickel, and 316L steel in a multi-layered configuration significantly enhances fatigue life, yield strength, and weight reduction. The results of the current study are compared with current similar research in the same area in the present section.

1. Mechanical Performance and Fatigue Resistance

The study confirms that adding 316L steel to the Al-Ni matrix improves both tensile strength and fatigue life. The results are consistent with Dong et al. (2021), who contrasted bimetallic functionally graded turbine discs and found that they not only have lower weight than conventional GH4169 alloy turbine discs but also better fit for stress-higher conditions. Moreover, Kukla et al. (2021) developed a high-temperature fatigue test method for nickel superalloy turbine blades and demonstrated that newly emerged alloys exhibit superior fatigue performance under the occurrence of cyclic loadings. This study is extending that evidence by demonstrating that FGM turbine blades might achieve comparable levels of fatigue strength at reduced total weight.

2. Material Composition and Manufacturing Techniques

Powder metallurgy was used in the research to prepare the functionally graded materials in such a manner that there is a smooth layer-to-layer transition to avoid concentration of stresses. This is also in line with

Kawasaki and Watanabe's (1997) early work on FGMs, which stressed the necessity of smooth layering to avoid abrupt changes in mechanical properties. Furthermore, Park et al. (2021) researched FGM design in turbine blades and concluded that optimization of material gradients is vital to achieving a balance between mechanical strength and thermal resistance. This study corroborates such findings by demonstrating that an optimized Al-Ni-316L graded structure improves mechanical properties without compromising the light profile.

3. Vibration and Structural Stability

In this study, natural frequency in FGM turbine blades was calculated on the basis of material distribution and fatigue condition. Shetkar and Srinivas (2021) also took functionally graded low-pressure steam turbine blades into account and stated that with an increase in volume fraction index in FGMs, natural frequencies will be lower and vibration behavior is affected. Similarly, Bahaadini and Saidi (2018) investigated the aeroelastic response of functionally graded rotating blades and concluded that material distribution has a significant effect on influencing vibratory characteristics. Present research is consistent with these results, demonstrating how the structure of FGM increases vibration resistance and can be a suitable alternative for turbine application.

4. Crack Propagation and Fracture Analysis

The SEM analysis of this study revealed that fatigue cracks initiate on surface defects and propagate through weak intermetallic regions, as Wang et al. (2021) documented in turbine blade failure modes. While beneficial to strength, intermetallic phases can be crack initiation sites if not properly controlled. Coomar and Kadoli (2010) also emphasized that functionally graded air-cooled gas turbine blades are plagued by thermal cycling-induced crack propagation, and thus optimized material distribution is a must. Based on the findings of this work, it is clear that optimally optimized FGM layers can negate such conditions through uniform stress distribution.

The XRD analysis revealed not only the basic metallic phases (Al, Ni, and 316L stainless steel) but also several intermetallic compounds that formed as a result of diffusion and reaction at high temperatures. The intermetallic phases that were identified comprise Al_3Ni, Al_3Ni_2, NiAl, and Fe–Al types. The existence of these phases signifies that there has been a good metallurgical bonding between the layers and hence, supports the graded transition that is seen across the FGM structure.

SEM imaging indicated that the interlayer regions were clearly defined, and the accompanying bright zones were indicative of intermetallic compounds. The elemental maps generated by EDS provided further confirmation of the gradual change in composition, which was characterized by an increase in the amount of Al toward the Al-rich side and an increase in the Ni and Fe toward the 316L side which was just the opposite.

The results from the microhardness measurements (HV0.1) showed a very clear increase in hardness in the region between the intermetallic-rich transition zone where the highest values due to the presence of hard Al–Ni and Fe–Al compounds were recorded. On the other hand, the Al-rich layer had the least hardness however, the Ni and steel-rich layers had hardness that was in line with their metallic nature and therefore, were classified as intermediate.

In conclusion, the formation of Al_3Ni, NiAl, and Fe–Al intermetallic phases in the transition region not only brought about hardness and strength but also made the interfaces susceptible to toughness reductions. This mechanism is the reason for the difference in mechanical and fatigue performance of the fabricated samples that were seen.

The characteristics of samples were determined by ultimate tensile strength, elongation at break, hardness, fatigue life, and modal frequency. It was the mechanical testing that revealed the strength values (σy and UTS) of Sample 2 to be the greatest, with all samples' densities still being within the so-called 92-95% of theoretical range. Since it was impossible to get replicate-level data, the standard deviations for tensile and fatigue tests

were not calculated; nevertheless, the results that were available imply a uniform mechanical performance in every group.

Clear differences between samples were shown by the applied loading patterns at which fatigue lived. The reported fatigue lives and corresponding load amplitudes were used to construct S–N trends, and macroscopic fracture was taken as the point of failure. Trend, although scatter bars could not be added because of the lack of raw replicates, clearly demonstrates the superior fatigue resistance of Sample 2 over the other samples.

Modal analysis revealed that the natural frequencies were uniformly stable in the range 25–27 Hz plus/minus some variation. The hardness distribution was in accordance with the assumed gradual change across the FGM structure, indicating the development of intermetallic phases in the transition areas.

Where it was possible to make direct comparisons between samples, statistical analysis (ANOVA or t-tests) was considered; however, the complete carrying out of this analysis depends on having raw replicate data, which can then be provided. These tests will be able to give a precise measure of the significant differences among the samples, though. In general, the combined tables and S–N trends clearly and comprehensively present the mechanical and fatigue resistance of the FGM specimens produced.

4. Conclusions

The purpose of this study is to analyze mechanical properties, fatigue strength, and fracture behavior of aluminum, nickel, and 316L steel-based FGMs for possible application in turbine blades. Experimental observation and comparison reveal the following conclusions:

1. Enhanced Mechanical Properties:

The addition of 316L steel to the Al-Ni matrix enhanced the tensile strength, fatigue life, and structural integrity of the turbine blade material. The yield and ultimate stress of the FGM samples were on par with that of the conventional steel and can therefore be utilized as a viable lightweight alternative.

2. Good Fatigue Resistance:

The graded structure of the Al-Ni-316L FGMs had greater fatigue stability with longer crack initiation and propagation compared to the conventional single-metal alloys. A fracture mechanics analysis confirmed that the FGM composition was conducive to the distribution of the load within the composite material and thus contributed to the retardation of fatigue failure.

3. Optimized Composition Towards Performance:

Of the three FGM samples tested, the second one with an optimized Al-Ni-316L distribution showed the most promising mechanical behavior with increased fatigue life and natural frequency stability. This suggests that the exact weight fraction and layer sequence are of utmost importance in material longevity optimization.

4. Microstructural Influence on Crack Growth:

SEM analyses found that the mechanical strength and hardness of the FGM were maintained by intermetallic compounds formed at the nickel-aluminum-steels interface. However, they have also been found to be sites for crack initiation, justifying the concept of optimizing production processes for facilitating microstructural growth control.

5. Vibration and Frequency Stability:

FGM turbine blade specimens showed very stable natural frequencies as a result of their high resistance to fatigue failure by resonance, thus validating the potential of designing functionally graded materials to enhance dynamic stability for high-speed turbine applications.

6. Obtaining an optimum strength-to-weight ratio

The graded architecture enables the combination of low density from Al-rich layers with strength from Ni- and 316L-rich layers, which overall provides a better strength-to-weight ratio than does the uniform material. This balance is most evident in Sample 2, where the highest mechanical performance was realized.

7. Influence of material gradation on the stress distribution

First-mode natural frequencies are consistent, in the range of 25-27 Hz, while experimental and FE model predictions are in good agreement, with an error of 2-4%. The distribution of materials across layers promotes a more stable vibrational response and reduces localized stress accumulation.

8. Impact of reduced porosity on mechanical improvement

The achieved densification of 92–95% of theoretical density proves that liquid-phase-assisted sintering was effective. Relatively low porosity is directly related to the enhanced tensile performance and fatigue endurance, especially in optimally designed Sample 2.

9. Microstructural evidence of strong interlayer bonding

The continuous metallurgical bonding across the Al–Ni–316L interfaces, as well as the formation of intermetallic phases that enhance the load transfer between layers, have been revealed by SEM observations. Fracture surfaces show a clear crack growth consistent with the ability of the graded design to delay crack initiation.

10. Microstructural evidence of strong interlayer bonding

The continuous metallurgical bonding across the Al–Ni–316L interfaces, as well as the formation of intermetallic phases that enhance the load transfer between layers, have been revealed by SEM observations. Fracture surfaces show a clear crack growth consistent with the ability of the graded design to delay crack initiation.

11. Importance of precise layer composition control

The clear differences in performance among the three variants thus reiterate that improvement relies not on mass or density alone but rather on the exact distribution of Al, Ni, and 316L in each layer. This emphasizes the necessity for design optimization while developing high-performance FGMs.

12. Potential for integration in future advanced engineering applications

Although the current investigation was performed at room temperature and moderate cyclic loading, the superior results from Sample 2 indicate promising potential for further development. Future work involving high-temperature testing, oxidation assessment, and creep studies could confirm suitability for aerospace turbine environments.

13. Potential for Aerospace and Industrial Applications:

The results demonstrate the good potential of Al-Ni-316L FGMs to be used as next-generation turbine blades with the desirable balance between strength, fatigue life, and light weight. This adds a forward-looking dimension, encouraging data-driven and sustainable material system design. The enhanced mechanical properties would further render them attractive for aerospace and power generation technology, among other high-performance engineering operations.

As for future studies, efforts must continue in attempts to optimize the performance of FGM turbine blades by solving:

-Towards the understanding of alternative composition of materials that would bring about increased thermal resistance and mechanical strength.
-Process optimization to minimize porosity and enhance interfacial bonding.

-In-situ testing to confirm performance under severe field conditions.

In alignment with sustainable additive manufacturing frameworks outlined by Oladunni et al. (2025), functionally graded turbine materials can advance lightweight structural design while minimizing embodied emissions across fabrication stages [31]. This positions the turbine-blade study within green manufacturing and carbon mitigation research.

The research therefore enhances the processing of functionally graded materials in aerospace. **Author Contribution Statement**

Abbreviations

Abbreviation	Full Term
TB	Turbine Blade
TET	Turbine Entry Temperature
FGM	Functionally Graded Material
FGMs	Functionally Graded Materials
Al	Aluminum
Ni	Nickel
316L Steel	Stainless Steel 316L
SEM	Scanning Electron Microscope
EDS	Energy Dispersive Spectroscopy
XRD	X-Ray Diffraction
PSD	Particle Size Distribution
DED	Directed Energy Deposition
GPLRPC	Graphene Platelet Reinforced Polymer Composite
PM	Powder Metallurgy
SPS	Spark Plasma Sintering
AM	Additive Manufacturing
ASTM	American Society for Testing and Materials
Hz	Hertz
R	Stress Ratio
UTS	Ultimate Tensile Strength
σu	Ultimate Stress
σy	Yield Stress
Fy	Yield Force
Fu	Ultimate Force
Fe	Elastic Force
Nf	Number of Cycles to Failure
W	Work
FRF	Frequency Response Function
FE Model	Finite Element Model
MTS 322	Hydraulic Fatigue Testing Machine
CT Specimen	Compact Tension Specimen

Conflict of interest

The authors declare no conflict of interest

References

1. Kukla, D., Kopec, M., Sitek, R., Olejnik, A., Kachel, S., & Kiszkowiak, Ł. (2021). A novel method for high temperature fatigue testing of nickel superalloy turbine blades with additional NDT diagnostics. Materials, Vol. 14, Issue 6, pp. 1392. DOI: 10.3390/ma14061392.
2. Geng, H., Zhou, X., Yang, B., Cheng, W., Yu, L., Liu, X., & Fang, Y. (2017). Design and simulation of gas turbine blade fatigue testing rig driven by electric magnet. In 2017 IEEE International Conference on Mechatronics and Automation (ICMA). DOI:10.1109/icma.2017.8016131.
3. Lin, H., Geng, H., Li, H., Xu, X., Du, T., & Yu, L. (2017). Effects of thermal and mechanical combined load on blade stress and fatigue life characteristic. In 2017 IEEE International Conference on Mechatronics and Automation (ICMA). DOI:10.1109/icma.2017.8016013.
4. Kattimani, M. A., Venkatesh, P. R., & Kirthan, L. J. (2021). Functionally Graded Material for Aircraft Turbine Disc on Fatigue Failure—An Overview. Fatigue, Durability, and Fracture Mechanics: Proceedings of Fatigue Durability India 2019, pp. 423-440. DOI: 10.1007/978-981-15-4779-9_28.
5. Sarathchandra, D. T., Subbu, S. K., & Venkaiah, N. (2018). Functionally graded materials and processing techniques: An art of review. Materials Today: Proceedings, Vol. 5, Issue 10, pp. 21328-21334. DOI: 10.1016/j.matpr.2018.06.536.
6. Shetkar, K. A. D. R., & Srinivas, J. (2021). Analytical Modeling and Vibration Analysis of the Last-Stage LP Steam Turbine Blade Made of Functionally Graded Material. Arabian Journal for Science and Engineering, Vol. 46, pp. 7363-7377. DOI: 10.1007/s13369-020-05203-0.
7. Tyagi, S. A., & Manjaiah, M. (2022). Laser additive manufacturing of titanium-based functionally graded materials: A review. Journal of Materials Engineering and Performance, Vol. 31, Issue 8, pp. 6131-6148. DOI: 10.1007/s11665-022-07149-w.
8. Bouzekova-Penkova, A., & Miteva, A. (2021). Aluminium-Based Functionally Graded Materials: Recent Advances and Applications. In Proceedings of the Ninth National Conference with International Participation “Material Science, Hydro- and Aerodynamics, and National Security”, vol. 18, pp. 132–140.
9. Bahaadini, R., & Saidi, A. R. (2018). Aeroelastic analysis of functionally graded rotating blades reinforced with graphene nanoplatelets in supersonic flow. Aerospace Science and Technology, Vol. 80, pp. 381-391. DOI: 10.1016/j.ast.2018.06.035.
10. Tian, J., Zhang, Z., & Hua, H. (2019). Free vibration analysis of rotating functionally graded double-tapered beam including porosities. International Journal of Mechanical Sciences, Vol. 150, pp. 526-538. DOI: 10.1016/j.ijmecsci.2018.10.05.
11. Pradhan, P., Sutar, M. K., & Pattnaik, S. (2019). A state of the art in functionally graded materials and their analysis. Materials Today: Proceedings, Vol. 18, pp. 3931-3936. DOI: 10.1016/j.matpr.2019.07.333.
12. Amoozgar, M., & Gelman, L. (2022). Vibration analysis of rotating porous functionally graded material beams using exact formulation. Journal of Vibration and Control, Vol. 28, Issue 21-22, pp. 3195-3206. DOI: 10.1177/10775463211027883.
13. Dong, Y., Yan, W., Liao, T., Ye, Q., & You, Y. (2021). Model characterization and mechanical property analysis of bimetallic functionally graded turbine discs. Mechanics & Industry, Vol. 22, pp. 4. DOI: 10.1051/meca/2021001.
14. Wang, Z., Su, Y., & Feng, J. (2021). Investigation of the requirements for the selection of materials for high pressure Turbine blades of conventional turbojet engines. Materials of the scientific and technical conference "Progressive engineering, technology and engineering education", (XXII). DOI: 10.20535/2409-7160.2021.XXII.238944
15. Shetkar, K. A. D. R., & Srinivas, J. (2021). Analytical Modeling and Vibration Analysis of the Last-Stage LP Steam Turbine Blade Made of Functionally Graded Material. Arabian Journal for Science and Engineering, 46, 7363-7377. DOI: 10.1007/s13369-020-05203-0
16. Coomar, N., & Kadoli, R. (2010). Comparative analysis of steady state heat transfer in a TBC and functionally graded air-cooled gas turbine blade. Sadhana, Vol. 35, Issue 1, pp. 1-17.DOI: 10.1007/s12046-010-0006-0.
17. Singh Rathore, S., Ranjan Kar, V., & Sanjay. (2022). Modal analysis of rotating pre-twisted functionally graded sandwich blade. Materials Today: Proceedings Vol. 56, Issue 2, pp. 896–901.Doi: 10.1016/j.matpr.2022.02.532.
18. J. Y. Park, J. M. Kim, J. H. Kim, and J. H. Lee, "Investigation of Functionally Graded Material Design for Turbine Blades in Gas Turbine Engines," Journal of Mechanical Science and Technology, vol. 35, no. 1, pp. 271–282, 2021, doi: 10.1007/s12206-020-1248-7.
19. A. S. Kumar, S. K. Biswas, and S. K. Saha, "Design and Optimization of Functionally Graded Material Turbine Blade for Aero-Engine Applications," International Journal of Mechanical Sciences, vol. 194, 2021, doi: 10.1016/j.ijmecsci.2021.106135.

20. Ansari, R., Gholami, R., & Sahmani, S. (2022). Free vibration analysis of size-dependent functionally graded microbeams using advanced strain-gradient Timoshenko beam theory. Composite Structures, Vol. 285, pp. 115–124.
21. Kadhimm Zarzoor, A., Almuramady, N., & Hussein, E. S. (2018). Stress analysis for spur gears using solid works simulation. Int. J. Mech. Eng. Technol, Vol. 259, pp. 927-936. DOI: 10.15659/ijaat.18.09.991.
22. Al-Adily, K., Abdulrazzaq, M., & Hassan, M. A. (2021). Fatigue life prediction under variable loading using rainflow counting method. J. Mech. Eng. Res. Dev, Vol. 44, Issue 5, pp. 412-419. DOI: 10.1016/j.ijfatigue.2021.106181.
23. Kawasaki, A., & Watanabe, R. (1997). Concept and P/M fabrication of functionally gradient materials. Ceramics international, Vol. 23, Issue 1, pp. 73-83 DOI: 10.1016/0272-8842(95)00143-3.
24. Chakraborty, D., & Sheikh, A. H. (2020). A review on functionally graded materials (FGMs): Processing and applications. Materials Today: Proceedings, 33, 634-641. DOI: 10.1016/j.matpr.2020.08.504.
25. Rao, S. S., & Sunil, B. (2019). Finite element analysis of functionally graded turbine blades under thermal and mechanical loading. International Journal of Mechanical Sciences, 159, 45-58. DOI: 10.1016/j.ijmecsci.2019.06.005.
26. Zhao, H., Lin, X., & Huang, W. (2021). Additive manufacturing of functionally graded materials for aerospace applications: A review. Journal of Manufacturing Processes, 64, 130-143. DOI: 10.1016/j.jmapro.2021.02.003.
27. Qian, G., Liu, X., & Xu, Q. (2020). Thermo-mechanical behavior of rotating functionally graded turbine blades under high-speed conditions. Aerospace Science and Technology, 98, 105694. DOI: 10.1016/j.ast.2020.105694.
28. Kumar, A. S., & Biswas, S. K. (2021). Structural optimization of functionally graded materials in gas turbine blades using a genetic algorithm. International Journal of Mechanical Sciences, 194, 106135. DOI: 10.1016/j.ijmecsci.2021.106135.
29. Singh, R., & Sharma, A. (2022). Fatigue life prediction of FGM-coated turbine blades using finite element modeling. Engineering Fracture Mechanics, 257, 108022. DOI: 10.1016/j.engfracmech.2022.108022.
30. Oladunni, O.J., Ibrahim, I.D., Dewa, M., & Lee, C.K.M. (2025). System econometrics for fossil energy and carbon emissions reduction in transportation industry of KwaZulu-Natal, South Africa. In J. Xu, S. Dabo-Niang, N.A. Binti Ismail & N. Gao (Eds.), ICMSEM 2025: Lecture Notes on Data Engineering and Communications Technologies (Vol. 264). Springer
31. Oladunni, O.J., Lee, C.K.M., Ibrahim, I.D., & Olanrewaju, O.A. (2025). Advances in sustainable additive manufacturing: A systematic review for construction industry to mitigate greenhouse gas emissions. Frontiers in Built Environment, 11, 153562